

Drops on soft solids: Free energy and double transition of contact angles

L. A. LUBBERS¹, J. H. WEIJS¹, L. BOTTO²,
S. DAS³, B. ANDREOTTI⁴, AND J. H. SNOEIJER¹

¹ Physics of Fluids Group, Faculty of Science and Technology, MESA+ Institute, University of Twente, 7500 AE Enschede, The Netherlands.

² Imperial College London, Department of Chemical Engineering, South Kensington Campus, London SW7 2AZ, UK

³ Department of Mechanical Engineering, University of Alberta, Edmonton, Alberta, Canada T6G 2G8

⁴ Physique et Mécanique des Milieux Hétérogènes, UMR 7636 ESPCI -CNRS, Univ. Paris-Diderot, 10 rue Vauquelin, 75005, Paris, France

(Received ?? and in revised form ??)

The equilibrium shape of liquid drops on elastic substrates is determined by minimising elastic and capillary free energies. The problem is governed by three length scales: the size of the drop R , the molecular size a , and the ratio of surface tension to elastic modulus γ/E . We show that the contact angles undergo two transitions upon changing the substrates from rigid to soft. The microscopic wetting angles deviate from Young's law when $\gamma/Ea \gg 1$, while the apparent macroscopic angle only changes in the very soft limit $\gamma/ER \gg 1$. Details of the elastic deformations are worked out in the simplifying case where the surface energy of the solid is assumed independent of the elastic strain. The total free energy is found to be lowest on softer substrates, consistent with recent experiments. Finally, we discuss how the variational framework can be generalized to properly account for surface stress.

1. Introduction

A liquid drop can deform a soft elastic substrate due to capillary forces (Lester 1961; Rusanov 1975, 1978; Shanahan 1987; de Gennes *et al.* 2004; Pericet-Camara *et al.* 2008). Elastic deformations take place over a length on the order of the elastocapillary length γ/E , where γ is the liquid surface tension and E the solid Young's modulus. Recent experiments have considered liquids on very soft elastomers with γ/E of the order of 1-100 microns and have reported many interesting features, such as the geometry near the contact line (Pericet-Camara *et al.* 2008; Jerison *et al.* 2011; Style *et al.* 2013a), compression of the solid (Marchand *et al.* 2012a), evaporation and spreading dynamics (Carre *et al.* 1996; Li *et al.* 2007; Pericet-Camara *et al.* 2008; Sokuler *et al.* 2010), as well as migration of droplets on substrates with a stiffness gradient (Style *et al.* 2013b).

While the contact angle of a drop on a rigid homogeneous substrate is governed by Young's law, the contact angle selection for a drop on a soft deformable substrate is still debated. One of the earliest theoretical approaches consisted of treating the elastic energy stored below the contact line as an effective line tension (Shanahan 1987; White 2003; Style & Dufresne 2012). This predicts an increase of the apparent, macroscopic contact angle on soft surfaces, which has been contradicted by recent experiments (Style *et al.* 2013a). The line tension approach did not include the surface energy of the solid, which turns out to be a crucial factor for the shaping of soft solids. Such surface effects were introduced by Jerison *et al.* (2011) and Limat (2012) in a purely macroscopic

theory based on the balance of forces exerted “on” the contact line. In this framework, the microscopic contact angles always obey Neumann’s law, regardless of E , as if the substrate at the contact line was a liquid. The same work reveals that there exists a transition for the apparent macroscopic contact angle, controlled by the dimensionless parameter γ/ER , where R is the drop size. By contrast, a microscopic description based on van der Waals interactions (Marchand *et al.* 2012*b*) suggests that Young’s law for the microscopic contact angle is recovered for $\gamma/Ea \ll 1$, where a is the characteristic length of molecular interactions. The formation of a solid cusp below the contact line arises for $\gamma/Ea \gg 1$, and the corresponding contact angles generically differ from Neumann’s law, even for very soft substrates.

The controversy on the selection of contact angles on soft substrates directly results from the difference between macroscopic and microscopic descriptions of capillarity. Our aim here is to revisit this question from a thermodynamic perspective. The lack of a consistent picture partly originates from the difficulty of defining a force balance near the contact line (Marchand *et al.* 2011). Also, the surface stress Υ (force per unit length) which is manifested in the superficial layers of a solid is different from the surface free energy γ (energy per unit area). This is due to the coupling of elastic strain and surface free energy, an effect that is absent for liquid-liquid interfaces and usually ignored in elasto-capillary modeling. Surface stress and surface energy are related by a thermodynamic law known as the Shuttleworth equation (Shuttleworth 1950):

$$\Upsilon = \gamma + \frac{d\gamma}{d\epsilon_{\parallel}}, \quad (1.1)$$

where ϵ_{\parallel} is the elastic strain parallel to the interface. The strain dependence $d\gamma/d\epsilon_{\parallel}$ is directly responsible for tangential elastic displacements around a contact line (Das *et al.* 2011; Marchand *et al.* 2012*a*; Weijs *et al.* 2013). Though the terminology surface stress is employed by Style *et al.* (2013*a*), their mechanical approach of the contact angle selection is not based on a consistent description that accounts for in-plane displacements.

Given the equilibrium nature of the problem and the thermodynamic relation (1.1), an alternative route is to consider the problem through variational calculus. Considering a semi-infinite elastic solid in a two-dimensional system, the elastic free energy per unit length can be expressed as a surface integral (Long *et al.* 1996):

$$\mathcal{F}_{el} = \frac{E}{2} \int_{-\infty}^{\infty} \frac{dq}{2\pi} \hat{Q}(q) \left[\hat{h}(q)\hat{h}(-q) + \hat{u}(q)\hat{u}(-q) \right], \quad (1.2)$$

where $\hat{h}(q)$ and $\hat{u}(q)$ are Fourier transforms of the normal and tangential displacements, $h(x)$ and $u(x)$, at the interface. The Green’s function reads $\hat{Q}(q) = 2|q|/3$ in the incompressible limit. The challenge is to derive the contact angles directly by minimising capillary and elastic free energies, i.e. without relying on a mechanical view in terms of a force balance. An important question then is whether microscopic and macroscopic descriptions of capillarity will give consistent results.

In this paper we for the first time compute the full shape of drops on elastic surfaces. This is done using a variational approach, exploring substrates from perfectly rigid (no deformation) to extremely soft (no elasticity). We predict the angles θ , θ_{SV} and θ_{SL} as defined in Fig. 1*a*, as a function of the “softness parameters” γ/Ea and γ/ER . In this work, we restrict ourselves to the case where the Shuttleworth-effect is absent, i.e. $d\gamma/d\epsilon_{\parallel} = 0$, for which the tangential deformations vanish. Even within this approximation, it is shown that both parameters govern a transition from Young’s law to Neumann’s law, but apply to different features of the angles in Fig. 1. This reveals the connection

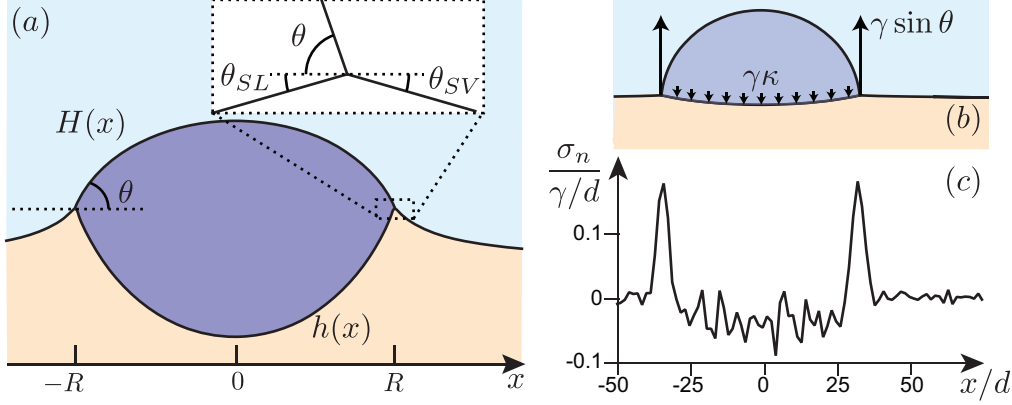


FIGURE 1. Drop on a soft solid. (a) The liquid and solid surface shapes are described by $H(x)$ and $h(x)$ respectively. The contact line geometry is characterized by the angles θ , θ_{SV} and θ_{SL} (see inset). (b,c) Normal component of capillary stress exerted on the solid. (b) Macroscopic view given by Eq. (2.13). A force per unit length is pulling on the solid at the contact line positions while a Laplace pressure is applied below the drop. (c) Microscopic view of the normal stress σ_n , as measured below a Lennard-Jones nanodroplet in Molecular Dynamics (adapted from Weijs *et al.* (2013)). The pulling force near the contact lines is spread over a finite width a , of a few molecular sizes (horizontal units expressed in molecular size d). At the center of the drop one recognizes the slightly negative capillary stress.

between previously proposed results in a single framework. In addition, we show how the free energy evolves with the stiffness and point out the connection to experiments of drop motion on substrate exhibiting a stiffness gradient (Style *et al.* 2013b).

2. Equilibrium conditions from variational analysis

2.1. Macroscopic theory of capillarity

2.1.1. A single contact line

We analyze a two-dimensional drop as sketched in Fig. 1. The liquid-vapor interface is described by $H(x)$, while $h(x)$ is the profile of the solid surface. When useful, we will use the index h_{SL} or h_{SV} to distinguish if the solid is wet or dry, with corresponding surface free energies γ_{SL} and γ_{SV} .

Before analysing the droplet, we consider the simpler case of a single contact line, located at $x = R$. The total capillary free energy can then be expressed as:

$$\mathcal{F}_c = \gamma \int_{-\infty}^R dx (1 + H'^2)^{1/2} + \gamma_{SL} \int_{-\infty}^R dx (1 + h_{SL}'^2)^{1/2} + \gamma_{SV} \int_R^{\infty} dx (1 + h_{SV}'^2)^{1/2}. \quad (2.1)$$

We anticipate a slope discontinuity $h_{SV}' \neq h_{SL}'$ at the contact line $x = R$. By definition of the contact line, H , h_{SL} and h_{SV} take the same value at $x = R$. This condition can be enforced by introducing two Lagrange multipliers λ_{SL} , λ_{SV} , which can be interpreted as reaction forces per unit length. The functional to be minimised becomes

$$\mathcal{F}_{tot} = \mathcal{F}_{el} + \mathcal{F}_c + \lambda_{SL} [H(R) - h_{SL}(R)] + \lambda_{SV} [H(R) - h_{SV}(R)], \quad (2.2)$$

where \mathcal{F}_{el} is as in (1.2). The minimization must be performed with respect to the fields $H(x)$, $h(x)$, and the contact line position R . As explained, the tangential displacements $u(x)$ vanish when the surface free energies are assumed constant (independent of the elastic strain).

First, we consider the variation $\delta H(x)$, which gives

$$\delta \mathcal{F}_{tot} = \delta H(R) \left[\lambda_{SL} + \lambda_{SV} + \frac{\gamma H'}{(1 + H'^2)^{1/2}} \right] + \int_{-\infty}^R dx \delta H(x) [-\gamma \kappa]. \quad (2.3)$$

The boundary term $\delta H(R)$ originates from the constraints on the contact line position and from the integration by parts of the capillary term \mathcal{F}_c with respect to $\delta H'$ and gives $\lambda_{SL} + \lambda_{SV} = \gamma \sin \theta$. This expression can be interpreted as the vertical force balance of a corner of liquid located at the contact line. The second term on the right-hand side gives the curvature $\kappa = H''/(1 + H'^2)^{3/2}$, which for a single contact line is equal to zero.

Second, we consider the variation $\delta h(x)$, which gives

$$\begin{aligned} \delta \mathcal{F}_{tot} = & \delta h_{SL}(R) \left[-\lambda_{SL} + \frac{\gamma_{SL} h'_{SL}}{(1 + h'^2_{SL})^{1/2}} \right] + \delta h_{SV}(R) \left[-\lambda_{SV} - \frac{\gamma_{SV} h'_{SV}}{(1 + h'^2_{SV})^{1/2}} \right] \\ & + \int_{-\infty}^R dx \delta h_{SL}(x) [-\gamma_{SL} \kappa_{SL}] + \int_R^{\infty} dx \delta h_{SV}(x) [-\gamma_{SV} \kappa_{SV}] \\ & + \int_{-\infty}^{\infty} dx \delta h(x) \left[E \int_{-\infty}^{\infty} \frac{dq}{2\pi} \widehat{Q}_n(q) \hat{h}(q) e^{iqx} \right], \end{aligned} \quad (2.4)$$

where the first terms are analogous to those in (2.3), but they now express vertical forces acting on a corner of solid. The last term represents the inverse Fourier transform of the variation of \mathcal{F}_{el} , and involves the elastic normal stress

$$\sigma_n(x) \equiv E \int_{-\infty}^{\infty} \frac{dq}{2\pi} \widehat{Q}_n(q) \hat{h}(q) e^{iqx}. \quad (2.5)$$

In principle, this elastic stress could contribute to the boundary condition at $x = R$, in case σ_n consists of a Dirac δ -function at $x = R$. Within the macroscopic framework, this can be excluded on a mathematical ground. As $\widehat{Q} \sim |q|$, a Dirac contribution of elasticity would require a (weakly) singular displacement, $h \sim \log |x - R|$, and hence a (weakly) diverging elastic free energy. The equilibrium condition at the contact line is therefore determined by the surface energies only (Jerison *et al.* 2011; Limat 2012), implying a weaker singularity in the form of a discontinuity in h' . Indeed, one can show that this implies a weakly diverging stress, $\sigma_n \sim \log |x - R|$, but an integrable free energy. Given this stress singularity, we emphasize that the physical answer to this question may be significantly different. We will come back later on the microscopic cutoff.

Following for now the rigorous macroscopic derivation, the variations at the contact line $\delta h(R)$ determine the Lagrange multipliers, $\lambda_{SL} = \gamma_{SL} \sin \theta_{SL}$, and $\lambda_{SV} = \gamma_{SV} \sin \theta_{SV}$. Combined with the boundary condition resulting from (2.3) these expressions give a relation between the contact angles,

$$\gamma \sin \theta = \gamma_{SL} \sin \theta_{SL} + \gamma_{SV} \sin \theta_{SV}, \quad (2.6)$$

which can be recognized as the vertical component of the Neumann condition. This boundary condition is analogous to that describing a liquid lens floating on another liquid, since the elastic energy does not give a contribution at the contact line in this case. The mechanical equilibrium away from the solid can be obtained by combining the integrals in (2.4), giving

$$\sigma_n(x) = \gamma_{SL} \kappa_{SL} \Theta(R - x) + \gamma_{SV} \kappa_{SV} \Theta(x - R) \equiv \gamma_s(x) \frac{h''}{(1 + h'^2)^{3/2}}, \quad (2.7)$$

where $\Theta(x)$ is the Heaviside step-function. This expression is not defined at $x = R$, where

instead it is replaced by a boundary condition (2.6). For $x \neq R$, the stress σ_n balances the Laplace pressure due to curvature κ_{SL} (κ_{SV}) of the wet (dry) solid interface.

Third, we consider variations of the contact line position δR . This variation receives contributions from the integration limits in \mathcal{F}_c , from the contact line constraints (terms involving $\lambda_{SL} + \lambda_{SV}$), but once again not from the energy contribution \mathcal{F}_{el} . The total variation (to be evaluated at $x = R$) gives:

$$\begin{aligned} \delta \mathcal{F}_{tot} &= \delta R \left\{ \gamma (1 + H'^2)^{1/2} + \gamma_{SL} (1 + h_{SL}'^2)^{1/2} - \gamma_{SV} (1 + h_{SV}'^2)^{1/2} \right. \\ &\quad \left. + (\lambda_{SV} + \lambda_{SL}) H' - \lambda_{SL} h_{SL}' - \lambda_{SV} h_{SV}' \right\} \\ &= \delta R \left\{ \frac{\gamma}{(1 + H'^2)^{1/2}} + \frac{\gamma_{SL}}{(1 + h_{SL}'^2)^{1/2}} - \frac{\gamma_{SV}}{(1 + h_{SV}'^2)^{1/2}} \right\}, \end{aligned} \quad (2.8)$$

where we used the previously obtained values for the Lagrange multipliers λ_{SL} and λ_{SV} . The individual terms can straightforwardly be expressed in terms of the angles defined in Fig. 1, and the second boundary condition for the contact angles becomes:

$$\gamma \cos \theta + \gamma_{SL} \cos \theta_{SL} = \gamma_{SV} \cos \theta_{SV}, \quad (2.9)$$

which can be recognized as the horizontal Neumann condition.

To summarize, we recover the usual Laplace pressure condition for the liquid interface $H(x)$. The solid interface shape $h(x)$ follows from the balance (2.7) of elastic stress σ_n and solid Laplace pressure. The problem is closed by the vertical and horizontal Neumann conditions (2.6, 2.9), serving as boundary conditions for the angles at the contact line.

2.1.2. A two-dimensional drop

We now consider a two-dimensional drop with contact lines at $x = R$ and $x = -R$. The expression for the free energy is similar to that for a single contact line, except that we have to consider two dry domains, $x > R$ and $x < -R$, and one wet domain $-R < x < R$. In addition, minimization is done at constant drop volume V , which is achieved by adding to the total energy a Lagrange multiplier term:

$$\mathcal{F}_V = P \left[V - \int_{-R}^R dx (H(x) - h(x)) \right]. \quad (2.10)$$

The newly added constraint does not contribute to the boundary condition, since $H(x) - h(x) = 0$ at $x = \pm R$, and hence we recover (2.6, 2.9). However, the constraint does introduce a contribution in the equilibrium equations for $H(x)$ and $h(x)$, which are:

$$-\gamma \kappa = P, \quad \sigma_n(x) = -P \Theta(|R - x|) + \gamma_s(x) \frac{h''}{(1 + h'^2)^{3/2}}. \quad (2.11)$$

The first relation requires the liquid interface to have a constant curvature, corresponding to the Laplace pressure $P = \gamma \sin \theta / R$. The second equation shows that P also acts as external stress on the boundary of the elastic medium below the drop. It is instructive to incorporate the vertical boundary condition (2.6) in the elastic stress, as

$$\sigma_n = \gamma \sin \theta f_n(x) + \left(\frac{\gamma_s(x) h'}{(1 + h'^2)^{1/2}} \right)', \quad (2.12)$$

where $f_n(x)$ is the distribution of normal stress due to the capillary forces,

$$f_n(x) = \delta(x - R) + \delta(x + R) - \frac{1}{R} \Theta(|R - x|). \quad (2.13)$$

This corresponds to the classical mechanical view of normal forces as depicted in Fig. 1b, consisting of two localized forces pulling upwards at the contact line, and a Laplace pressure pushing downward below the drop. Indeed, one can show that the Dirac- δ at the contact line balances with the γ_s -term in (2.12), recombining to (2.6).

2.2. Microscopic theory of capillarity

In the limit of perfectly rigid solids one would expect to recover Young's law. However, the purely macroscopic theory derived above shows that the wetting angles are given by the Neumann conditions *regardless of stiffness*, which is clearly unphysical. Also, we showed that the elastic stress is singular at the contact line. These artefacts of the purely macroscopic approach are due to the assumption of perfectly localized line forces, represented by δ -functions in (2.13). In reality, capillary forces are spread out over a finite width a , typically a few nanometers, because the interface is diffuse at the molecular level and due to the finite range of van der Waals interactions. This finite width is illustrated in Fig. 1c, showing the normal stress exerted by a nanodroplet on an elastic substrate as measured in a Molecular Dynamics simulation (Weijs *et al.* 2013).

The finite width of the interface can be taken into account in a truly microscopic description, using a disjoining pressure (White 2003) or Density Functional Theory (Das *et al.* 2011; Marchand *et al.* 2012b). Here we propose a simplified model that captures the essence of these microscopic models, but yet allows for a numerical solution with realistic separation of microscopic scale ($a \sim \text{nm}$) and macroscopic scale ($R \sim \text{mm}$). Namely, we retain the boundary condition (2.9), but represent the line forces in (2.13) by a function g of finite width

$$f_n(x) = \frac{1}{a}g\left(\frac{x-R}{a}\right) + \frac{1}{a}g\left(\frac{x+R}{a}\right) - \frac{1}{R}\Theta(|R-x|). \quad (2.14)$$

For our numerical solutions, g is chosen as a normalized Gaussian; other choices give similar results. As we will show, the contact angles display two distinct transitions that are governed by the parameters $\gamma/(Ea)$ and $\gamma/(ER)$.

2.3. Dimensionless equations and solution strategy

Solving for $h(x)$ from (2.12) is challenging, owing to the integral nature of σ_n , the discontinuity in $\gamma_s(x)$ and the presence of non-linear terms. Following Style & Dufresne (2012) and Limat (2012), we choose to simplify the problem by considering the case $\gamma_{SV} = \gamma_{SL} = \gamma_s$, and assume $h'^2 \ll 1$ to linearize the last term in (2.12). The latter condition is ensured by choosing moderate values of γ/γ_s . We then solve the resulting equation by applying a Fourier transform. In the remainder we rescale all lengths by R and the pressure by γ/R . The macroscopic model then depends on two dimensionless parameters: $\gamma/(ER)$ and γ/γ_s . The microscopic model has an additional parameter, namely $\tilde{a} = a/R$, or equivalently $\gamma/(Ea)$. Solving for the solid profile in Fourier space $\hat{h}(q)$ [Eq. (2.12)] gives:

$$\hat{h}(q) = \frac{\gamma}{ER} \sin \theta \left\{ \frac{\hat{f}_n(q, \tilde{a}) \hat{\mathcal{K}}(q)}{1 + \frac{\gamma}{ER} \frac{\gamma_s}{\gamma} q^2 \hat{\mathcal{K}}(q)} \right\}, \quad (2.15)$$

where

$$\hat{f}(q, \tilde{a}) = 2 \left(e^{-\frac{1}{2}(\tilde{a}q)^2} \cos q - \frac{\sin q}{q} \right), \quad \text{and} \quad \hat{\mathcal{K}}(q) \equiv \hat{Q}^{-1}(q) = \frac{3}{2|q|}. \quad (2.16)$$

The macroscopic theory corresponds to $\tilde{a} = 0$. Numerical solutions for $h(x)$ that satisfy (2.9) are obtained iteratively, by adjusting θ . Typical results are shown in Fig. 2.

$$\gamma/ER = 10^{-2} \longrightarrow \gamma/ER = 10^{-1} \longrightarrow \gamma/ER = 10^0 \longrightarrow \gamma/ER = 10^1$$

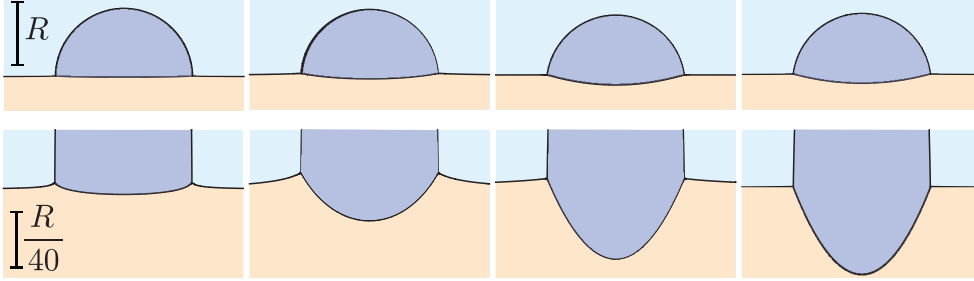


FIGURE 2. Simulated shapes of the drop (dark blue) and of the solid substrate (light orange) for different values of γ/ER , $\gamma/\gamma_s = 0.3$, $\tilde{a} = 0$. Top: As the solid becomes softer (increasing γ/ER) the drop sinks increasingly deeper in the substrate. Bottom: Zoom near the contact line region, with the vertical scale stretched 40 times. The elevation at the contact line first increases for increasing softness, but on further increasing the softness the elevation subsequently decreases.

3. Numerical results

3.1. Microscopic and macroscopic contact angles: two transitions

We now describe how the wetting angles depend on the stiffness of the substrate. It is important to distinguish between the microscopic wetting angles θ_S , θ_{SL} , θ_{SV} (Fig. 3), and the macroscopic angle θ (Fig. 1a). The former angles reveal the microscopic geometry of the contact line region, while the latter is the apparent angle of the spherical cap with respect to the undeformed substrate. The results presented in Fig. 3 are obtained for $\gamma/\gamma_s = 0.1$, $\tilde{a} = 10^{-5}$, and Young's angle $\theta_Y = 90^\circ$ (since $\gamma_{SV} = \gamma_{SL}$).

Our key finding is that the wetting angles undergo two transitions when changing the softness parameter. For $\gamma/Ea \ll 1$, in the perfectly rigid limit, the microscopic solid angle is unchanged, *i.e.*, $\theta_S = 180^\circ$, while the liquid angle $\theta = \theta_Y$ is equal to Young's angle. A first transition arises for $\gamma/Ea \sim 1$: the solid angle changes and the geometry evolves towards a Neumann cusp. This transition is quantified in the plot in Fig. 3, where the solid line on the left measures the solid deflection $\pi - \theta_S = \theta_{SV} + \theta_{SL}$, for different values of softness. The relationship between the microscopic angles evolves from Young's law to Neumann's law. The Neumann cusp, as predicted in the macroscopic theory for all values of the stiffness, is only recovered for $\gamma/Ea \gg 1$.

The angle θ also displays a transition. As long as $\gamma/ER \ll 1$, this angle is unaffected by elastic deformations, which are visible only in a narrow zone near the contact line. The macroscopic angle changes only once the scale of the deformation γ/E becomes comparable to the drop size R , *i.e.* when $\gamma/ER \sim 1$. In the very soft limit the angle saturates, reaching the value expected for a liquid lens. Microscopically, this transition constitutes a rotation by angle ϵ of the Neumann geometry, by an angle ϵ (Fig. 3, top). This transition is quantified by the solid line on the right in Fig. 3, middle.

For completeness, we also carried out the macroscopic analysis for three-dimensional axisymmetric drops. The analysis is analogous to that in the two-dimensional case, except that the axisymmetric elastic stress $\sigma_n(r)$ can now be calculated using a Hankel transform (Style & Dufresne 2012). However, as we here self-consistently determine the value of the angle θ , we are for the first time able to assess the validity of the “elastic line tension” argument (White 2003; Style & Dufresne 2012). The result for the deflection angle ϵ is shown as the dashed line in Fig. 3, from which it is apparent that this angle is almost indistinguishable from that obtained in the two-dimensional case. The trend

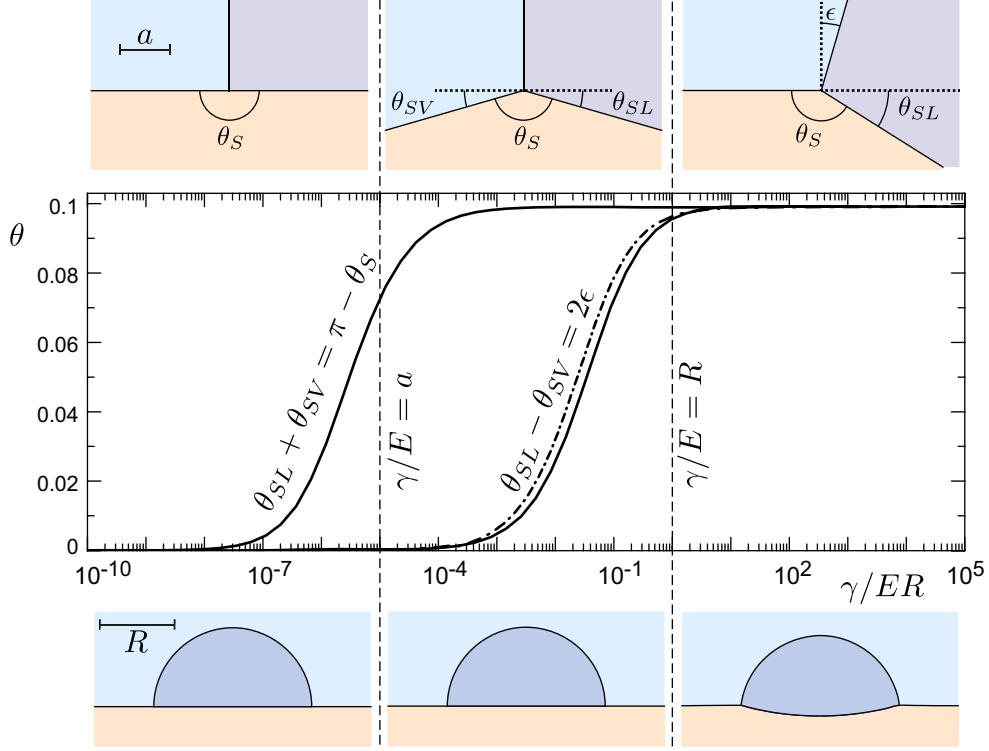


FIGURE 3. Double transition of contact line angles, for 2D drops (solid) and 3D drops (dashed). The substrate stiffness is varied by modifying the softness parameters γ/ER , at fixed $\gamma/\gamma_s = 0.1$ and $\tilde{a} = 10^{-5}$. The left curve refers to the deviation of the solid angle, $\pi - \theta_S$, showing the development of the solid cusp. The right hand curves give the cusp rotation angle ϵ , defined from the microscopic wetting angles shown in the top panel (scale a). The bottom panel shows the corresponding macroscopic drops shapes. This shows that (i) the microscopical geometry of the contact line first develops a Neumann-like cusp when γ/E is of the order of the microscopic scale a and (ii) the macroscopic angle of the drop is altered only when γ/E reaches the size of the drop R .

for θ , decreasing when reducing the stiffness, is *opposite* to that predicted by considering line tension, but in agreement with recent experiments by Style *et al.* (2013a).

3.2. Elevation of the contact line and total energy vs. softness

While varying γ/ER we observe that the elevation of the contact line for the macroscopic model ($\tilde{a} = 0$) evolves non-monotonically (cf. Fig. 2). This is quantified in Fig. 4, showing the contact line elevation $h(x/R = 1)$ as a function of γ/ER : The contact line elevation $h(1)$ has a maximum for $\gamma/ER \sim 0.1$. In the stiff limit ($E \rightarrow \infty$) the solid opposes any stress without deforming while in the soft limit ($E \rightarrow 0$) the geometry of the drop-substrate interface is identical to that of a floating liquid lens. From the numerical results we find that the contact line height fits closely to

$$h(1) \sim \left(\frac{\gamma}{ER}\right) \ln(\gamma/ER), \quad \text{and} \quad h(1) \sim \left(\frac{\gamma}{ER}\right)^{-1} \ln(ER/\gamma), \quad (3.1)$$

for small and large γ/ER , respectively. The behaviour in the rigid limit was previously discussed by Limat (2012), who showed that for weak deformations that the solid surface tension provides a natural regularization of the logarithmic divergence at the contact line.

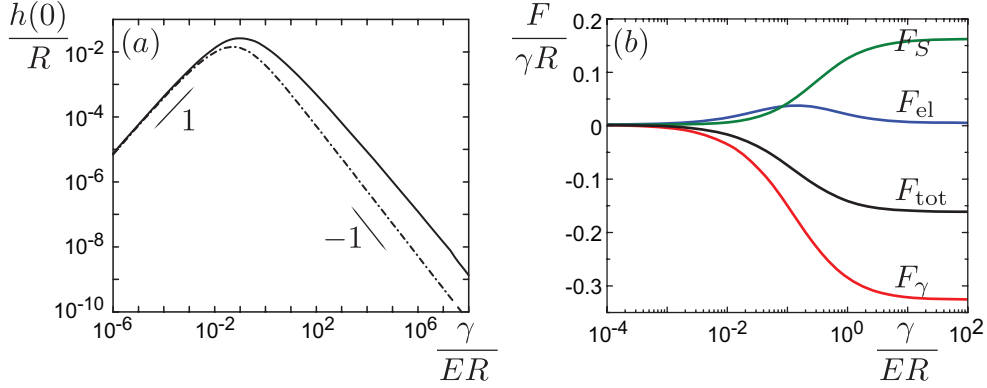


FIGURE 4. Nonmonotonic elevation at the contact line and free energy as function of softness. (a) Elevation at the contact line as function of the softness parameter (γ/ER) for $\gamma/\gamma_s = 0.1$: solid lines are results from 2-D theory, dash-dotted lines from 3-D theory. Deformations at the contact line are nonmonotonic with the softness parameter and display a maximum deformation around $\gamma/ER = 0.1$, as seen also in Fig. 2. (b) Changes in elastic energy \mathcal{F}_{el} , capillary solid energy \mathcal{F}_S , and capillary liquid energy \mathcal{F}_γ , as function of the softness parameter for $\gamma/\gamma_s = 0.5$. The model predicts a decrease in total free energy as the softness increases. A drop on a infinitely rigid substrate ($E = 0$) was used as the reference case.

The dashed line, which refers to the three-dimensional drop, suggests a $h \sim (\gamma/ER)^{-1}$ dependence for $\gamma/ER \gg 1$.

Finally, we calculate the elastic energy (\mathcal{F}_{el}), the solid capillary energy (\mathcal{F}_S), and the liquid capillary energy (\mathcal{F}_γ) for a droplet on a substrate of varying stiffness [see Fig. 4(b)]. For these calculations, the droplet volume was kept constant for all values of γ/ER . This allows for a direct comparison with recent experiments by Style *et al.* (2013b) where droplets were found to move to softer regions on a substrate with a stiffness gradient. Our numerics provide an explanation for this result, with a lower total free energy $\mathcal{F}_{tot} \equiv \mathcal{F}_{el} + \mathcal{F}_S + \mathcal{F}_\gamma$ for droplets on softer substrates. The energies \mathcal{F}_{el} and \mathcal{F}_S are actually increasing for softer surfaces, but by a smaller amount than the gain in liquid-vapor capillary energy (\mathcal{F}_γ).

4. Discussion

In this work, we have calculated the shapes of drops on soft substrates by minimization of the elastic and capillary energies. We find that in addition to the drop size R and the elastocapillary length γ/E , a third length-scale is required in order to fully describe elastocapillary interactions: The molecular scale a . This extra length scale is crucial for describing the Young to non-Young transition that occurs for sessile droplets on progressively softer substrates. In addition, the regularization is necessary to avoid a singularity of elastic stress at the contact line. Such a singular tendency implies that, generically, the substrates will be deformed beyond the linear elastic regime – one expects strain hardening and even plasticity (Limat 2012) – which up to present have never been taken into account. Another key ingredient for future work is to take into account the strain-

dependence of the surface free energies, which lead to tangential elastic displacements (Weijs *et al.* 2013).

REFERENCES

- CARRE, A., GASTEL, J. C. & SHANAHAN, M. E. R. 1996 Viscoelastic effects in the spreading of liquids. *Nature* **379** (6564), 432–434.
- DAS, S., MARCHAND, A., ANDREOTTI, B. & SNOEIJER, J. H. 2011 Elastic deformation due to tangential capillary forces. *Phys. Fluids* **23** (7), 072006.
- DE GENNES, P.-G., BROCHARD-WYART, F. & QUERE, D. 2004 *Capillarity and wetting phenomena: drops, bubbles, pearls, waves*. Springer, New York.
- JERISON, E. R., XU, Y., WILEN, L. A. & DUFRESNE, E. R. 2011 Deformation of an Elastic Substrate by a Three-Phase Contact Line. *Phys. Rev. Lett.* **106** (18), 186103.
- LESTER, G. R. 1961 Contact angles of liquids at deformable solid surfaces. *J. Colloid Sci.* **16** (4), 315.
- LI, G., GRAF, K., BONACCURSO, E., GOLOVKO, D. S., BEST, A. & BUTT, H.-J. 2007 Evaporation structures of solvent drops evaporating from polymer surfaces: Influence of molar mass. *Macromolecular Chemistry and Physics* **208** (19-20), 2134–2144.
- LIMAT, L. 2012 Straight contact lines on a soft, incompressible solid. *Eur. Phys. J. E* **35** (12), 134.
- LONG, D., AJDARI, A. & LEIBLER, L. 1996 Static and dynamic wetting properties of thin rubber films. *Langmuir* **12** (21), 5221–5230.
- MARCHAND, A., DAS, S., SNOEIJER, J. H. & ANDREOTTI, B. 2012 Capillary pressure and contact line force on a soft solid. *Phys. Rev. Lett.* **108**, 094301.
- MARCHAND, A., DAS, S., SNOEIJER, J. H. & ANDREOTTI, B. 2012 Contact Angles on a Soft Solid: From Young’s Law to Neumann’s Law. *Phys. Rev. Lett.* **109** (23), 236101.
- MARCHAND, A., WEIJS, J. H., SNOEIJER, J. H. & ANDREOTTI, B. 2011 Why is surface tension a force parallel to the interface? *Am. J. Phys.* **79** (10), 999–1008.
- PERICET-CAMARA, R., BEST, A., BUTT, H.-J. & BONACCURSO, E. 2008 Effect of capillary pressure and surface tension on the deformation of elastic surfaces by sessile liquid micro-drops: An experimental investigation. *Langmuir* **24** (19), 10565–10568.
- PERICET-CAMARA, R., BONACCURSO, E. & GRAF, K. 2008 Microstructuring of polystyrene surfaces with nonsolvent sessile droplets. *ChemPhysChem* **9** (12), 1738–1746.
- RUSANOV, A. I. 1975 Theory of wetting of elastically deformed bodies .1. Deformation with a finite contact-angle. *Colloid J. USSR* **37** (4), 614–622.
- RUSANOV, A. I. 1978 Thermodynamics of deformable solid-surfaces. *J. Colloid Interface Sci.* **63** (2), 330–345.
- SHANAHAN, M. E. R. 1987 The influence of solid micro-deformation on contact-angle equilibrium. *J. Phys. D-Appl. Phys.* **20** (7), 945–950.
- SHUTTLEWORTH, R. 1950 The surface tension of solids. *Proc. Phys. Soc., London Sect. A* **63** (365), 444–457.
- SOKULER, M., AUERNHAMMER, G. K., ROTH, M., LIU, C., BONACCURSO, E. & BUTT, H.-J. 2010 The softer the better: Fast condensation on soft surfaces. *Langmuir* **26** (3), 1544–1547.
- STYLE, R. W., BOLTANSKIY, R., CHE, Y., WETTLAUFER, J. S., WILEN, L. A. & DUFRESNE, E. R. 2013a Universal deformation of soft substrates near a contact line and the direct measurement of solid surface stresses. *Phys. Rev. Lett.* **110**, 066103.
- STYLE, R. W., CHE, Y., PARK, S. J., WEON, B. M., JE, J. H., HYLAND, C., GERMAN, G. K., POWER, M. P., WILEN, L. A., WETTLAUFER, J. S. & DUFRESNE, E. R. 2013b Patterning droplets with durotaxis. *Proc. Natl. Acad. Sci. U.S.A.* .
- STYLE, R. W. & DUFRESNE, E. R. 2012 Static wetting on deformable substrates, from liquids to soft solids. *Soft Matter* **8** (27), 7177–7184.
- WEIJS, J. H., ANDREOTTI, B. & SNOEIJER, J. H. 2013 Elasto-capillarity at the nanoscale: on the coupling between elasticity and surface energy in soft solids. *Soft Matter* **9**, 8494–8503.
- WHITE, L. R. 2003 The contact angle on an elastic substrate. 1. The role of disjoining pressure in the surface mechanics. *J. Colloid Interface Sci.* **258** (1), 82–96.